AGU PUBLICATIONS

Geophysical Research Letters

RESEARCH LETTER
10.1002/2015GL065043

Key Points:
- Internal wave VKE spectra have universal shape (different from GM), independent of f, N, ...
- Dissipation-normalized VKE spectra collapse tightly, conflicting with Gregg-Henyey-Polzin scaling
- We present a simple new VKE-based fine structure parameterization for turbulence accurate to factor 2

Correspondence to:
A. M. Thurnherr,
ant@ldeo.columbia.edu

Citation:
Thurnherr, A. M., E. Kunze, J. M. Toole, L. St. Laurent, K. J. Richards, and A. Ruiz-Angulo (2015), Vertical kinetic energy and turbulent dissipation in the ocean, *Geophys. Res. Lett.*, *42*, 7639–7647, doi:10.1002/2015GL065043.

Received 24 JUN 2015
Accepted 27 AUG 2015
Accepted article online 2 SEP 2015
Published online 21 SEP 2015

Vertical kinetic energy and turbulent dissipation in the ocean

A. M. Thurnherr[1], E. Kunze[2], J. M. Toole[3], L. St. Laurent[3], K. J. Richards[4], and A. Ruiz-Angulo[5]

[1]Lamont-Doherty Earth Observatory, Columbia University, Palisades, New York, USA, [2]NorthWest Research Associates, Bellevue, Washington, USA, [3]Woods Hole Oceanographic Institution, Woods Hole, Massachusetts, USA, [4]Department of Oceanography, University of Hawai'i at Mānoa, Honolulu, Hawaii, USA, [5]Centro de Ciencias de la Atmósfera, Universidad Nacional Autónoma de México, México D. F., Mexico

Abstract Oceanic internal waves are closely linked to turbulence. Here a relationship between vertical wave number (k_z) spectra of fine-scale vertical kinetic energy (VKE) and turbulent dissipation ϵ is presented using more than 250 joint profiles from five diverse dynamic regimes, spanning latitudes between the equator and 60°. In the majority of the spectra VKE varies as k_z^{-2}. Scaling VKE with $\sqrt{\epsilon}$ collapses the off-equatorial spectra to within $\sqrt{2}$ but underestimates the equatorial spectrum. The simple empirical relationship between VKE and ϵ fits the data better than a common shear-and-strain fine-scale parameterization, which significantly underestimates ϵ in the two data sets that are least consistent with the Garrett-Munk (GM) model. The new relationship between fine-scale VKE and dissipation rate can be interpreted as an alternative, single-parameter scaling for turbulent dissipation in terms of fine-scale internal wave vertical velocity that requires no reference to the GM model spectrum.

1. Introduction

The global thermohaline overturning circulation of the ocean redistributes heat across our planet and plays a fundamental role in the climate system [e.g., *Marshall and Speer*, 2012]. In order to close this overturning circulation and maintain the density stratification of the deep ocean, diapycnal mixing is required [e.g., *Munk*, 1966; *Munk and Wunsch*, 1998; *Wunsch and Ferrari*, 2004]. Away from boundaries, the turbulent kinetic energy dissipation rate ϵ covaries with fine-scale [O(10 m)] shear and strain variances [*Gregg*, 1989; *Polzin et al.*, 1995], consistent with predictions of internal wave/wave interaction theory [*McComas and Müller*, 1981; *Henyey et al.*, 1986] for a cascade from longer to shorter scales where waves break to produce turbulence. This relationship between internal wave properties and turbulence forms the basis of a parameterization for turbulent dissipation in terms of fine-scale shear and strain variances [*Polzin et al.*, 1995; *Gregg et al.*, 2003], which we term Gregg-Henyey-Polzin (GHP) scaling. Applying GHP scaling to oceanographic data involves multiple difficult approximations and assumptions [*Polzin et al.*, 2014].

The primary result of our study is finding a robust empirical relationship between fine-scale internal wave vertical kinetic energy (VKE) and turbulent dissipation rate (ϵ) using more than 250 profiles of vertical velocity w_{ocean} and ϵ collected during four oceanographic cruises in five locations (section 2). Vertical wave number (k_z) spectra of VKE from all locations vary as k_z^{-2} (section 3). VKE spectra from 10 to 60° latitude exhibit levels proportional to $\sqrt{\epsilon}$, and this scaling proves a better fit than GHP scaling in two of the data sets. Independent fits of the Garrett-Munk (GM) model to fine-scale shear and VKE spectra yield mutually inconsistent nondimensional spectral energy levels for the same two data sets. The close relationship between VKE and dissipation rate can be interpreted as a new scaling for turbulence based on fine-scale VKE with smaller biases albeit larger scatter than the GHP shear-and-strain parameterization. The main results are discussed in section 4.

2. Data and Methods

In order to investigate the relationship between VKE and turbulence, five data sets of vertical velocity (w_{ocean}) and microstructure-derived turbulent kinetic energy dissipation ($\epsilon_{\mathrm{micro}}$) are used (Tables 1 and 2). In all data sets, the corresponding microstructure and lowered acoustic Doppler current profiler/conductivity-temperature-depth (LADCP/CTD) measurements at a given depth are separated by a few hundred meters horizontally and by 20–30 min in time.

Table 1. Data Acquisition and Processing Parameters[a]

Data Set	Instruments	Profiles	Spectral Windows	dz_{bin}	$\lambda_{finescale}$
Equatorial thermocline	1 × WH600	104	125	2 m	40–160 m
East Pacific Rise	2 × WH300	36	446	8 m	150–320 m
Luzon Strait	2 × WH300	71	305	6 m	60–320 m
South Pacific	1 × WH300	48	517	8 m	70–320 m
Drake Passage	1 × WH300	8	168	8 m	70–320 m

[a]Data acquisition and processing parameters. WH300 and WH600 are Teledyne/RDI Workhorse ADCPs with 300 and 600 kHz transducer frequencies, respectively; for each data set, the total number of profiles and spectral windows are listed; dz_{bin} indicates ADCP bin/pulse lengths, and $\lambda_{finescale}$ indicates the range of vertical wavelengths included in the fine scale, with the short-wave limits determined from the spectra (see text for details).

Equatorial thermocline (MIXET project). During 2 weeks of sampling in October and November 2012, a thermocline (upper 300 m) time series of w_{ocean} and ϵ_{micro} was collected at a station at 156°E directly (within 50 m) on the equator [*Lee et al.*, 2014]. The LADCP data were collected in 2 m bins, using a downward looking 600 kHz acoustic Doppler current profiler (ADCP). Microstructure profiles were collected immediately after each LADCP/CTD cast with a tethered TurboMAP profiler. Many of the upcast LADCP velocities in this data set are contaminated by package wake effects.

East Pacific Rise (LADDER-3 cruise). During 2 weeks of sampling in November and December 2007, 36 joint profiles of w_{ocean} and ϵ_{micro} were collected in a region of modest turbulence near the crest of the East Pacific Rise (EPR) between 9°30′N and 10°N [*Thurnherr and St. Laurent*, 2011]. The LADCP data were collected in 8 m bins with a dual-head 300 kHz system. The microstructure data were collected simultaneously with the LADCP/CTD casts with an untethered Rockland Scientific VMP-6000 microstructure profiler.

Luzon Strait (IWISE project). During 2 weeks of sampling in June and July 2011, 71 joint profiles of w_{ocean} and ϵ_{micro} were collected in Luzon Strait near 121°45′E 20°15′N, a region of extreme internal wave activity and turbulence [*Alford et al.*, 2011]. The LADCP data were collected primarily in 6 m bins with a dual-head 300 kHz system. A VMP-6000 system was used to obtain microstructure measurements during the CTD/LADCP casts.

Drake Passage (DIMES US2 cruise). During 4 days of sampling in February and March 2010, eight profiles of w_{ocean} and ϵ_{micro} were collected between 58°S and 61°40′S along a section crossing Drake Passage near 66°W [*St. Laurent et al.*, 2012], another dynamically active region. The LADCP data used here were collected in 8 m bins with a 300 kHz downward looking ADCP. The microstructure data were collected simultaneously with the LADCP/CTD casts with three different untethered profilers, two Rockland Scientific VMP-6000s, and WHOI's HRP-2.

South Pacific (DIMES US2 cruise). Before occupying the Drake Passage section, during the same cruise and using the same instrumentation, 48 additional profiles of w_{ocean} and ϵ_{micro} were collected in the Pacific sector of the Southern Ocean (53–63°S 75–103°W) during 5 weeks of sampling in January and February 2010. In this region turbulence levels are low and middepth shear levels are consistent with the canonical Garret-Munk model [*Ledwell et al.*, 2011].

Table 2. Environmental Parameters[a]

Data Set	Latitude	Max(Depth) (m)	N (rad s^{-1}])	b (m)	k_z^* (rad m^{-1})
Equatorial thermocline	equator	240 (± 40)	$10.0\ (\pm 2.7) \times 10^{-3}$	100	0.2×10^{-2}
East Pacific Rise	9.7 (± 0.2)°N	2550 (± 380)	$2.2\ (\pm 1.1) \times 10^{-3}$	600	0.7×10^{-2}
Luzon Strait	20.2 (± 0.2)°N	1160 (± 260)	$5.4\ (\pm 2.6) \times 10^{-3}$	300	3.2×10^{-2}
South Pacific	58.9 (± 2.0)°S	2180 (± 620)	$1.9\ (\pm 0.9) \times 10^{-3}$	900	0.4×10^{-2}
Drake Passage	59.7 (± 1.4)°S	2870 (± 960)	$1.3\ (\pm 0.6) \times 10^{-3}$	1000	0.2×10^{-2}

[a]Environmental parameters (standard deviations in parentheses); data from the top 150 m of the water column are ignored; N is buoyancy frequency, b denotes stratification e-folding lengthscale, and k_z^* is the vertical wave number corresponding to the canonical GM bandwidth $j^* = 3$ (see text for details).

From the microstructure shear measurements, turbulent kinetic energy dissipation is estimated with standard methods [e.g., *Ledwell et al.*, 2011; *St. Laurent et al.*, 2012]. Additionally, shear-and-strain fine-scale dissipation rate estimates (ϵ_{GHP}) are calculated with Gregg-Henyey-Polzin scaling as implemented by *Kunze et al.* [2006]. The fine-scale spectra are calculated from standard 1 dbar averaged CTD profiles and from horizontal LADCP velocities derived with a reimplementation of the shear method [*Thurnherr*, 2012].

LADCP profiles of vertical ocean velocity w_{ocean} are obtained by subtracting vertical package velocity w_{CTD} from ADCP-derived vertical velocity measurements, before binning the resulting velocities in depth [*Thurnherr*, 2011]. The CTD data—only measurements collected with SeaBird 911plus systems are used here—are processed as follows. First, outliers in pressure, temperature, and conductivity, as well as pressure bias and spikes, are algorithmically removed from the raw 24 Hz CTD data. The cleaned-up time series are bin averaged into 6 Hz time series. Using standard methods, sound speed and CTD depth are derived; the latter are differentiated with respect to time to yield estimates of vertical package velocity, which are filtered in the frequency domain with a 2 s low-pass cutoff. The resulting 6 Hz time series of CTD depth, sound speed, and w_{CTD} are combined with the raw ADCP velocity measurements to produce separate downcast and upcast profiles of w_{ocean}. All profiles are gridded at 10 m vertical resolution, regardless of ADCP bin size.

After processing, the vertical velocities are quality controlled by visually inspecting various processing diagnostics, including pitch/roll time series, depth-binning statistics, and time lagging correlations. Except for the equatorial thermocline, the data sets from all regions contain a few profiles contaminated by dropped CTD scans caused by data transmission glitches between the CTD underwater unit and the deck box. As the recorded CTD scans are neither properly time stamped nor incrementally labeled, the number of dropped scans cannot be determined, resulting in clock offsets contaminating parts of the affected profiles. The contaminated vertical velocities are flagged. Several profiles from the equatorial thermocline and Luzon Strait have gaps, either because of insufficient acoustic scatterers at depth (equatorial thermocline) or because of package tilt angles exceeding 12° (Luzon Strait). Vertical velocity anomalies at the edges of these gaps are flagged as well. A subset of the profiles from the South Pacific and Luzon Strait shows highly variable vertical velocities in the upper few hundred meters of the water column, often with extreme vertical gradients. The association of some of the vertical velocity maxima with acoustic scattering layers suggests contamination by vertically moving organisms [e.g., *Fischer and Visbeck*, 1993]. Corresponding w_{ocean} anomalies are flagged.

VKE periodograms are calculated from the vertical velocity profiles by Fourier transforming the w_{ocean} measurements in half-overlapping windows at 10 m vertical resolution with means removed before transformation. 160 m thick windows are used for the short equatorial thermocline profiles, and 320 m thick windows are used for all other data. No periodograms are calculated for windows with flagged or missing velocities. Additionally, only the downcasts from the equatorial thermocline are used because of package wake contamination affecting many of the upcasts. In order to avoid biological and other near-surface contamination, data from depths <150 m are excluded from the analysis. Due to the coarse resolution, the bottom 100 m of the water column are not included in the analysis either. All available periodograms from a given window (up to four, from downward and upward looking ADCPs recording separate downcasts and upcasts) are averaged and corrected for attenuation at high wave numbers caused by ADCP range averaging and by vertical binning during processing [*Polzin et al.*, 2002; *Thurnherr*, 2012]. The short-wavelength (high wave number) cutoff for the resolved fine-scale range for each data set (Table 1) is determined visually from the data set-averaged spectra. For all data sets, the resolved scales are much greater than the corresponding typical Ozmidov scales—in the Luzon Strait data, where turbulence is strongest, 97% of all Ozmidov scale estimates are <10 m (not shown).

Internal wave LADCP/CTD observations are often compared to Garrett-Munk vertical wave number spectra of shear and strain, integrated over all frequencies between f and N [e.g., *Gregg and Kunze*, 1991]

$$\mathrm{GM}_{\mathrm{shear}}(k_z)[E_0, b, j^*] = \frac{3\pi}{2} E_0 b j^* \frac{k_z^2}{(k_z + k_z^*)^2} \tag{1}$$

$$\mathrm{GM}_{\mathrm{strain}}(k_z)[E_0, b, j^*] = \frac{\pi}{2} E_0 b j^* \frac{k_z^2}{(k_z + k_z^*)^2}, \tag{2}$$

where the nondimensional spectral energy level $E_0 = 6.3 \times 10^{-5}$; b is the stratification e-folding scale; j^* is the peak wave number (with energy rolling off toward higher and lower wave numbers), which quantifies the

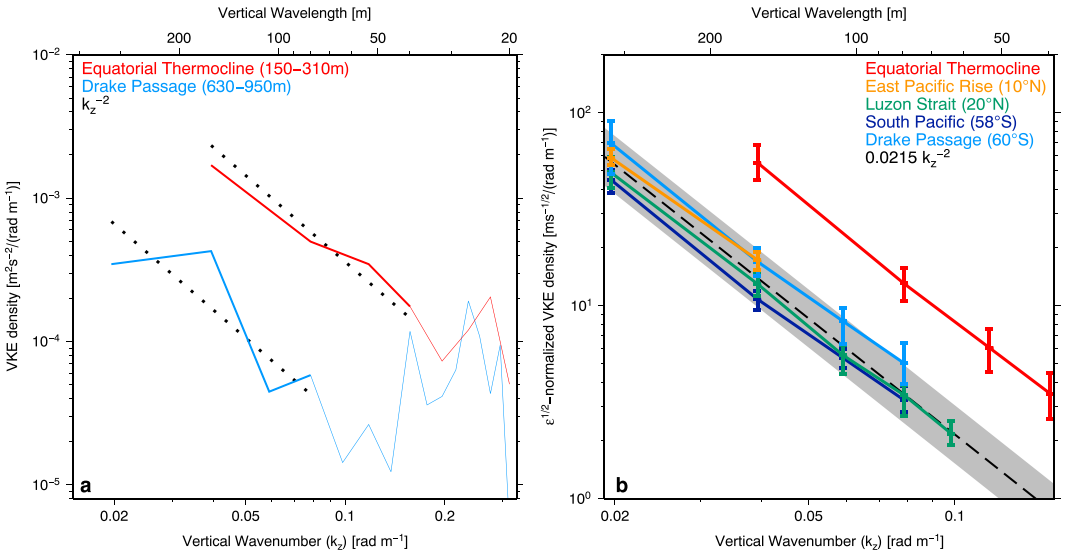

Figure 1. Vertical wave number (k_z) spectra of VKE. (a) Example spectra from individual profile windows (solid red and blue lines) with instrument-dependent resolved fine-scale ranges (Table 1) highlighted with heavier lines; dotted black lines show fine-scale k_z^{-2} power law fits. (b) $\sqrt{\epsilon}$-normalized, data set-averaged raw spectra, without the noise-dominated high wave number tails; error bars indicate 95% confidence intervals from bootstrapping; dashed line shows relationship (4), also normalized by $\sqrt{\epsilon}$, with shading corresponding to factor of 2 errors in ϵ.

bandwidth of the internal wave field; $k_z^* = j^*\pi N/(bN_0)$; and $N_0 = 5.3 \times 10^{-3}$ rad s^{-1} [*Gregg and Kunze*, 1991]. Here we also use the corresponding GM prescription for vertical wave number VKE spectral density

$$\mathrm{GM}_{\mathrm{VKE}}(k_z)[E_0, b, j^*, N, f] = \pi E_0 b N f j^* \frac{1}{(k_z + k_z^*)^2}, \tag{3}$$

noting the different latitudinal and stratification dependencies compared to expressions (1) and (2). Data set-averaged values for N, b, and k_z^* are listed in Table 2 where N and b are based on fits to the observed stratification profiles, independent of the w spectrum. Following common practice [e.g., *Kunze et al.*, 2006], we use the canonical Garret-Munk bandwidth parameter $j^* = 3$ to estimate k_z^*.

3. Results

Each of the five data sets (section 2) yields between 125 and 517 window-averaged spectra (1561 in total; Table 1) of internal wave VKE, which we write as $p(k_z)$. Most of the spectra are consistent with $p \propto k_z^{-2}$ up to a limiting vertical wave number O(0.1 rad m^{-1}) where the spectra flatten due to measurement noise (Figure 1a). The ensemble-averaged spectra from all five data sets are individually consistent with $p \propto k_z^{-2}$ (Figure 1b). The apparently universal k_z^{-2} spectral slope of VKE implies that a single-parameter model for internal wave VKE may be possible. In order to explore this possibility, a fine-scale VKE level is estimated for each spectrum by fitting a k_z^{-2} power law in the resolved fine-scale wave number band. The fit, illustrated in Figure 1a, is carried out in log-log space, and VKE is quantified by p_0, the resulting intercept (i.e., $p_0 = p(k_0) = p[\log k_z = 0]$, where $k_0 = 1$ rad m^{-1}, corresponding to a vertical wavelength $\lambda_0 = 2\pi$ m). Spectra with RMS differences between observed VKE spectral density and the corresponding power law fits exceeding log 0.4 m^2 s^{-1} (rad m)$^{-1}$ are discarded (≈30% of the available samples). The remaining p_0 from the off-equatorial data sets are correlated with the corresponding dissipation measurements, averaged over the same windows the spectra are calculated (Figure 2). Different averaging methods were explored. They all yield similar values, but the most consistent results are achieved with simple arithmetic averaging of all available measurements, which is the method used here. The equatorial data are not included in Figure 2 because they exhibit markedly different ratios between fine-scale VKE and dissipation rate (Figure 1b), qualitatively consistent with the findings of *Gregg et al.* [2003]. In order to test to what degree the off-equatorial data are described by a single power law, the p_0 values are averaged in equal-sized log ϵ bins, using bootstrapping to estimate uncertainties. The resulting averages (error bars in Figure 2) are consistent with a power law slope of $\frac{1}{2}$, the slope of the two line segments in the figure, implying that $p_0 \propto \sqrt{\epsilon}$ across nearly five decades of oceanic turbulence.

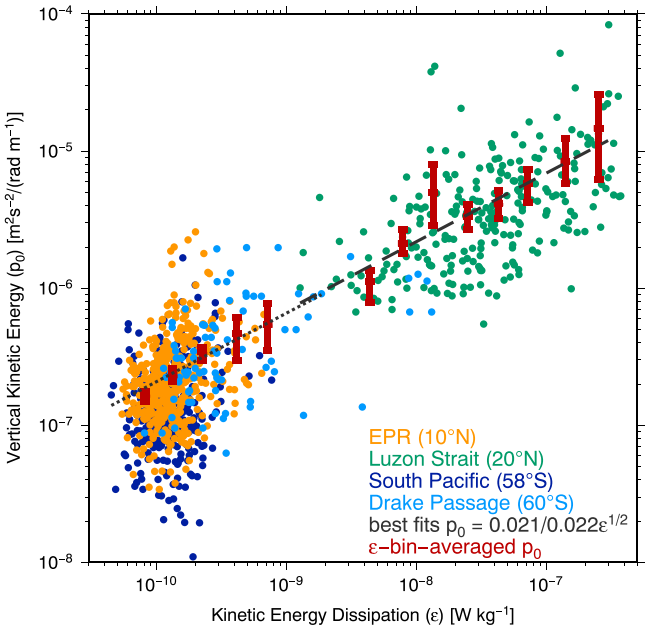

Figure 2. Internal wave VKE (p_0) versus kinetic energy dissipation (ϵ_{micro}). Error bars show p_0 averages in 0.1 wide log ϵ bins with ≥ 8 samples, with bootstrapping-derived uncertainties. The dotted and dashed lines show independent fits $p_0 \propto \sqrt{\epsilon}$ to two subsets of the data, yielding mutually consistent constants of proportionality 0.0215 ± 0.0005 s$^{-\frac{1}{2}}$; the dashed line shows a fit to the Luzon Strait samples with $\epsilon \leq 3 \times 10^{-7}$ W kg^{-1}; the dotted line shows a fit to the samples from the EPR, South Pacific, and Drake Passage with $\epsilon \leq 2 \times 10^{-9}$ W kg^{-1}; see text for details.

In order to quantify the relationship between p_0 and ϵ, the power law $p_0 = c\sqrt{\epsilon}$ is fit to two separate subsets of the data: a high-turbulence subset consisting only of Luzon Strait samples with $\epsilon \leq 3 \times 10^{-7}$ W kg^{-1} and a lower turbulence subset consisting of all samples from the EPR, South Pacific, and Drake Passage with $\epsilon \leq 2 \times 10^{-9}$ W kg^{-1}. The close agreement between the two independent fits to the raw data ($c_1 = 0.021$ s$^{-\frac{1}{2}}$ and $c_2 = 0.022$ s$^{-\frac{1}{2}}$, respectively, for the EPR/South Pacific/Drake Passage and for Luzon Strait) provides additional support for the notion of a single power law governing the relationship between p_0 and ϵ away from the equator.

Using $\sqrt{\epsilon}$ to normalize fine-scale VKE yields an algebraic expression for internal wave VKE power density in terms of vertical wave number and turbulent dissipation,

$$p(k_z, \epsilon) = c\epsilon^{\frac{1}{2}} k_z^{-2}, \tag{4}$$

with $c = c_1$ or $c = c_2$ from the fits described above. The dissipation-normalized data set-averaged raw spectra all agree with this algebraic prescription to better than a factor $\sqrt{2}$, except for the equatorial thermocline where observed VKE is elevated approximately fourfold (Figure 1b).

The Garrett-Munk model (section 2) provides an alternative prescription for internal wave VKE. In expression (3), VKE spectral density is only consistent with a k_z^{-2} power law for $k_z \gg k_z^*$. In the observations from Luzon Strait $p \propto k_z^{-2}$ is unambiguously valid at least down to $k_z \approx 2 \times 10^{-2}$ rad m^{-1} (Figure 1b), indicating that this criterion is violated since $k_z^*[j^* = 3] \approx 3 \times 10^{-2}$ rad m^{-1} in that region (Table 2). As a result, the curvature in the corresponding GM prescription for VKE at Luzon Strait is inconsistent with the observations unless j^* is set to its minimum value of 1 (not shown).

When $k_z \gg k_z^*$, expressions (3) and (4) can be equated to yield a formal scaling for dissipation in terms of the GM model parameters,

$$\epsilon \propto (E_0 b N f j^*)^2. \tag{5}$$

Together with GHP scaling ($\epsilon \propto \mathrm{KE}^2$), expression (5) indicates that $E_0 b N f j^*$ is a measure of internal wave VKE. Assuming a canonical $j^* = 3$ and using observational estimates for b, N, and f (Table 2), the GM model for

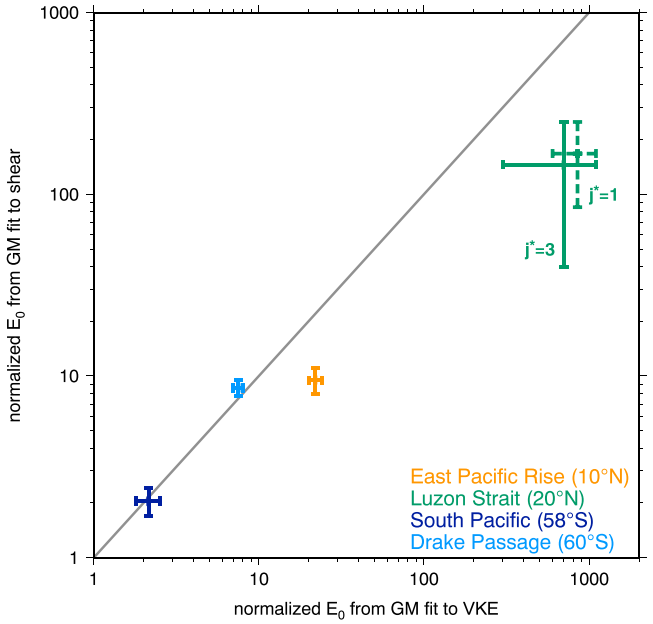

Figure 3. Estimates of the GM model parameter E_0 normalized by its reference value (6.3×10^{-5}) from fits of expressions (1) and (3) to data set-averaged observed spectra of shear and VKE, respectively, and plotted against each other. Error limits are from the model spectra bracketing the observations; solid and dashed lines indicate $j^* = 3$ and $j^* = 1$, respectively. The EPR and Luzon Strait data are inconsistent with the Garrett-Munk model; see text for details.

VKE (3) is fit separately to each data set-averaged VKE spectrum (Figure 1b), yielding a set of unique estimates for E_0, the only remaining free model parameter. When compared to an alternate set of E_0 estimates derived from fits of expression (1) to the shear spectra in the same data sets (Figure 3), agreement is found for the South Pacific and Drake Passage data, but the corresponding E_0 estimates disagree significantly for the East

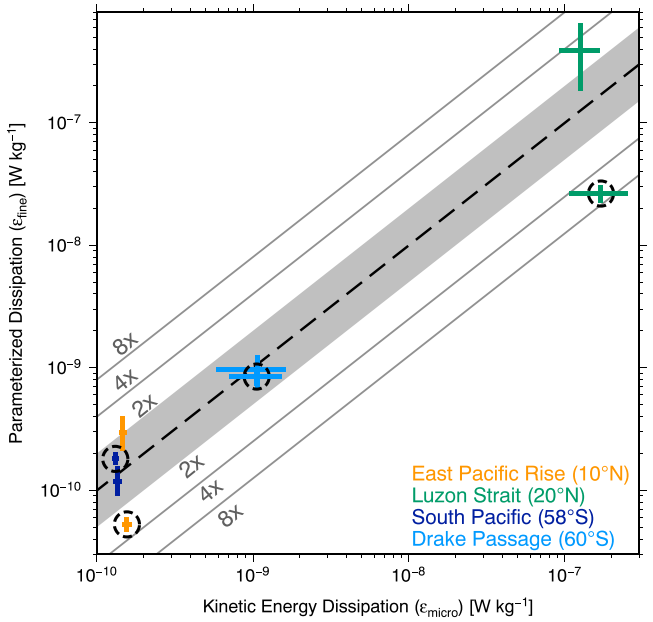

Figure 4. Fine structure- versus microstructure-derived kinetic energy dissipation, averaged for each data set, with error bars indicating 95% confidence intervals from bootstrapping. Estimates from Gregg-Henyey-Polzin scaling [*Kunze et al.*, 2006] are marked with dashed circles. The remaining (unmarked) samples are from the new VKE parameterization (6); method calibration and validation are based on independent subsets of the data; see text for details.

Pacific Rise and Luzon Strait data, with relatively more VKE compared to shear variance at both sites. Using $j^*=1$ does not improve agreement at Luzon Strait.

The quasi-universal VKE spectrum (4) can be expressed as a new fine-scale parameterization for turbulence

$$\epsilon_{\mathrm{VKE}} = (p_0/C)^2, \tag{6}$$

where $C = ck_0^{-2}$ and $k_0 = 1$ rad m^{-1}. In order to test this new parameterization, we use $c_1 = 0.021$ s$^{-\frac{1}{2}}$ (from the fit to the EPR, South Pacific, and Drake Passage data), to estimate ϵ_{VKE} in Luzon Strait, and $c_2 = 0.022$ s$^{-\frac{1}{2}}$ (from Luzon Strait) to estimate ϵ_{VKE} over the EPR, in the South Pacific, and in Drake Passage. The new parameterization yields dissipation rate estimates consistent within factor of 2 errors with the corresponding microstructure measurements (Figure 4). In contrast, the shear-and-strain Gregg-Henyey-Polzin scaling, as implemented by *Kunze et al.* [2006], yields EPR and Luzon Strait estimates that are biased low by factors of 3 and 7, respectively. On the other hand, the scatter (*y* axis error bars in Figure 4) of the shear-and-strain GHP estimates is significantly smaller than the corresponding scatter of the VKE-based estimates in all four off-equatorial data sets.

4. Discussion

In spite of the fact that two of our data sets are inconsistent with the Garrett-Munk model (Figure 3), the observations presented above are nevertheless consistent with prior inferences of a quasi-universal distribution of energy in the internal wave continuum, where wave-wave interactions support a downscale cascade resulting in turbulence and mixing. Our finding that off-equatorial turbulent dissipation ϵ scales as the square of VKE is consistent with the scaling predicted by internal wave/wave interaction theory and modeling [*McComas and Müller*, 1981; *Henyey et al.*, 1986; *Sun and Kunze*, 1999], as well as with comparisons between microstructure and fine-scale shear and strain levels [*Gregg*, 1989; *Wijesekera et al.*, 1993; *Polzin et al.*, 1995]. As some of our data do not conform to the GM model, we propose the empirical scaling (4) as the basis for a new fine-scale parameterization for ϵ in terms of VKE (6) since it appears to provide consistent estimates within a factor of 2 for latitudes spanning 10–60°. In contrast, Gregg-Henyey-Polzin scaling based on vertical wave number spectra of vertical shear and strain [*Gregg et al.*, 2003; *Kunze et al.*, 2006] underestimates turbulence in two (EPR and Luzon Strait) out of our four data sets. Because similar biases have been reported elsewhere [e.g., *Hibiya et al.*, 2012], we hypothesize that these biases are intrinsically associated with the shear-and-strain method rather than with any particular implementation. In addition to being associated with smaller biases, the new VKE parameterization is considerably simpler than shear-and-strain based methods, as it is based on w_{ocean} data alone and does not require any of the difficult and often uncertain corrections for latitude, shear-to-strain ratio (frequency content of the internal wave field), and buoyancy frequency required for the latter [*Polzin et al.*, 2014].

In our data from the equatorial thermocline, neither GHP scaling nor expression (6) adequately describes the relationship between internal wave kinetic energy and turbulence. GHP scaling predicts $\epsilon \to 0$ as the equator is approached, whereas (6) is independent of latitude. In our equatorial observations, the turbulence levels are suppressed by approximately factor 15 compared to the off-equatorial data at the same VKE; i.e., the observations lie between the two predictions. The observed suppression directly on the equator is qualitatively similar but considerably less strong than the factor ≈25–80× suppression inferred from shear/strain measurements within 1° of the equator [from *Gregg et al.*, 2003, Figure 1]. At higher latitudes, our results suggest two plausible reasons for the biases of the shear-and-strain method when applied to the Luzon Strait and EPR data. First, both data sets are inconsistent with the Garrett-Munk model (Figure 3) used to scale the observed spectral levels of shear and strain; i.e., the method biases may be related to GM model assumptions that are violated, as has been argued before [e.g., *Kunze et al.*, 2002; *Sheen et al.*, 2013; *Polzin et al.*, 2014; *Waterman et al.*, 2014]. Even for data that conform to the GM model, our analysis indicates inconsistency with GHP scaling, however. Assuming that the GM model holds, (5) implies that the dissipation rate $\epsilon \propto E_0^2 N^2 f^2$, which has different dependencies on f and N than GHP scaling, where $\epsilon \propto E_0^2 N^2 f \mathrm{arccosh}(N/f)$ [*Henyey et al.*, 1986]. This inconsistency, too, may be associated with violation of a GM model assumption, as there have been few prior measurements of w_{ocean}, which is dominated by high-frequency internal waves [*Voorhis*, 1968; *Desaubies*, 1975; *Pinkel*, 1975; *Eriksen*, 1978], with which to test the GM model's assumed separability in vertical wave number and frequency near N. As it seems plausible for the Earth's rotation to affect near-inertial and high-frequency waves differently, there may well be different latitudinal scalings for wave-wave interactions on different frequencies.

Independent of the details of our interpretation, the apparent inconsistencies found in the data illustrate that our understanding of the internal wave spectrum and the energy cascade from large-scale internal waves to turbulence production remains incomplete.

In general, it is not clear where the GM model applies and, thus, where GHP scaling can be expected to be accurate. Our data are inconsistent with the GM model not only in Luzon Strait, a region of large solitary wave generation and extreme turbulence [e.g., *Warn-Varnas et al.*, 2010; *Alford et al.*, 2011], but also over the EPR where internal wave and turbulence levels are much more moderate [*Thurnherr and St. Laurent*, 2011]. In contrast, we find that the profiles both from the open South Pacific, characterized by background levels of internal wave activity and turbulence [*Ledwell et al.*, 2011], and from Drake Passage, where internal waves and turbulence are strong [*St. Laurent et al.*, 2012], are consistent with the GM model and GHP scaling is accurate within a factor of 2. In contrast to GHP scaling, the new VKE parameterization applies even where the GM model does not. While our analysis does not reveal any reasons for the apparent universality of the relationship (4) between VKE and dissipation, we speculate that these two quantities may both represent products of internal wave/wave interaction.

Acknowledgments
Funding for collection of the data was provided by the National Science Foundation under grants OCE-0728766, OCE-0425361, and OCE-0424953 (LADDER); OCE-1029722 (MIXET); and OCE-0622630 (DIMES US2, supplemented with LDEO institutional funds), as well as by the Office of Naval Research under grant N00014-10-10315 (IWISE). Salary for the analysis was provided by NSF grants OCE-1030309 and OCE-1232962, supplemented with LDEO institutional support. Software and documentation for calculating w_{ocean} and ϵ_{VKE} profiles from LADCP/CTD data are available for download from http://www.ldeo.columbia.edu/LADCP. The processed profiles of vertical ocean velocity and the corresponding window-averaged dissipations used in this analysis are available on request from the corresponding author (e-mail: ant@ldeo.columbia.edu).

The Editor thanks two anonymous reviewers for their assistance in evaluating this paper.

References

Alford, M. H., et al. (2011), Energy flux and dissipation in Luzon Strait: Two tales of two ridges, *J. Phys. Oceanogr.*, *41*, 2211–2222.
Desaubies, Y. J. F. (1975), A linear theory of internal wave spectra and coherences near the Väisälä frequency, *J. Geophys. Res.*, *80*, 895–899.
Eriksen, C. C. (1978), Measurements and models of fine structure, internal gravity waves, and wave breaking in the deep ocean, *J. Geophys. Res.*, *83*, 2989–3009.
Fischer, J., and M. Visbeck (1993), Seasonal variation of the daily zooplankton migration in the Greenland Sea, *Deep Sea Res., Part I*, *40*, 1547–1557.
Gregg, M. C. (1989), Scaling turbulent dissipation in the thermocline, *J. Geophys. Res.*, *94*, 9686–9698.
Gregg, M. C., and E. Kunze (1991), Internal wave shear and strain in Santa Monica Basin, *J. Geophys. Res.*, *96*, 16,709–16,719.
Gregg, M. C., T. B. Sanford, and D. P. Winkel (2003), Reduced mixing from the breaking of internal waves in equatorial ocean waters, *Nature*, *422*, 513–515.
Henyey, F. S., J. Wright, and S. M. Flatté (1986), Energy and action flow through the internal wave field: An eikonal approach, *J. Geophys. Res.*, *91*, 8487–8495.
Hibiya, T., N. Furuichi, and R. Robertson (2012), Assessment of fine-scale parameterizations of turbulent dissipation rates near mixing hotspots in the deep ocean, *Geophys. Res. Lett.*, *39*, L24601, doi:10.1029/2012GL054068.
Kunze, E., L. K. Rosenfeld, G. S. Carter, and M. C. Gregg (2002), Internal waves in Monterey submarine canyon, *J. Phys. Oceanogr.*, *32*, 1890–1913.
Kunze, E., E. Firing, J. M. Hummon, T. K. Chereskin, and A. M. Thurnherr (2006), Global abyssal mixing inferred from lowered ADCP shear and CTD strain profiles, *J. Phys. Oceanogr.*, *36*, 1553–1576.
Ledwell, J. R., L. C. St. Laurent, J. B. Girton, and J. M. Toole (2011), Diapycnal mixing in the Antarctic Circumpolar Current, *J. Phys. Oceanogr.*, *41*, 241–246.
Lee, C., K.-I. Chang, J. H. Lee, and K. J. Richards (2014), Vertical mixing due to double diffusion in the tropical western Pacific, *Geophys. Res. Lett.*, *41*, 7964–7970, doi:10.1002/2014GL061698.
Marshall, J., and K. Speer (2012), Closure of the meridional overturning circulation through Southern Ocean upwelling, *Nat. Geosci.*, *5*, 171–180.
McComas, C. H., and P. Müller (1981), The dynamic balance of internal waves, *J. Phys. Oceanogr.*, *11*, 970–986.
Munk, W. (1966), Abyssal recipes, *Deep Sea Res.*, *13*, 707–730.
Munk, W., and C. Wunsch (1998), Abyssal recipes. II: Energetics of tidal and wind mixing, *Deep Sea Res.*, *45*, 1977–2010.
Pinkel, R. (1975), Upper ocean internal wave observations from Flip, *J. Geophys. Res.*, *80*, 3892–3910.
Polzin, K., E. Kunze, J. Hummon, and E. Firing (2002), The finescale response of lowered ADCP velocity profiles, *J. Atmos. Oceanic Technol.*, *19*, 205–224.
Polzin, K. L., J. M. Toole, and R. W. Schmitt (1995), Finescale parameterizations of turbulent dissipation, *J. Phys. Oceanogr.*, *25*, 306–328.
Polzin, K. L., A. C. Naveira Garabato, T. N. Huussen, B. M. Sloyan, and S. Waterman (2014), Finescale parameterizations of turbulent dissipation, *J. Geophys. Res. Oceans*, *119*, 1383–1419, doi:10.1002/2013JC008979.
Sheen, K. L., et al. (2013), Rates and mechanisms of turbulent dissipation and mixing in the Southern Ocean: Results from the Diapycnal and Isopycnal Mixing Experiment in the Southern Ocean DIMES, *J. Geophys. Res. Oceans*, *118*, 2774–2792, doi:10.1002/jgrc.20217.
St. Laurent, L., A. C. Naveira Garabato, J. R. Ledwell, A. M. Thurnherr, J. M. Toole, and A. J. Watson (2012), Turbulence and diapycnal mixing in Drake Passage, *J. Phys. Oceanogr.*, *42*, 2143–2152.
Sun, H., and E. Kunze (1999), Internal wave-wave interactions. Part II: Spectral energy transfer and turbulence production, *J. Phys. Oceanogr.*, *29*, 2905–2919.
Thurnherr, A. M. (2011), Vertical velocity from LADCP data, *Proceeding, CWTMC'11 (IEEE)*, Monterey, Calif.
Thurnherr, A. M. (2012), The finescale response of lowered ADCP velocity measurements processed with different methods, *J. Atmos. Oceanic Technol.*, *29*, 597–600.
Thurnherr, A. M., and L. C. St. Laurent (2011), Turbulence and diapycnal mixing over the East Pacific Rise crest near 10°N, *Geophys. Res. Lett.*, *38*, L15613, doi:10.1029/2011GL048207.
Voorhis, A. D. (1968), Measurements of vertical motion and the partition of energy in the New England slope water, *Deep Sea Res.*, *15*, 599–608.
Warn-Varnas, A., J. Hawkins, K. G. Lamb, S. Piacsek, S. Chin-Bing, D. King, and G. Burgos (2010), Solitary wave generation dynamics at Luzon Strait, *Ocean Modell.*, *31*, 9–27.

Waterman, S., K. L. Polzin, A. C. Naveira Garabato, K. L. Sheen, and A. Forryan (2014), Suppression of internal wave breaking in the Antarctic Circumpolar Current near topography, *J. Phys. Oceanogr.*, *44*, 1466–1492.

Wijesekera, H., L. Padman, T. Dillon, M. Levine, C. Paulson, and R. Pinkel (1993), The application of internal-wave dissipation models to a region of strong mixing, *J. Phys. Oceanogr.*, *23*, 269–286.

Wunsch, C., and R. Ferrari (2004), Vertical mixing, energy, and the general circulation of the oceans, *Annu. Rev. Fluid Mech.*, *36*, 281–314.